Tracking the dispersal of river water, atmospheric deposition, and shallow sedimentary trace metal inputs from the Congo region into the South Atlantic

Yuanyuan Gu[1], Mark James Hopwood[1], Dustin Carroll[2], Te Liu[3], Stephan Krisch[4]

[1]Department of Ocean Science and Engineering, Southern University of Science and Technology, Shenzhen, China

[2]Moss Landing Marine Laboratories, San José State University, California, USA

[3]School of Ocean & Earth Science, University of Southampton, Southampton, UK

[4]Technical University of Braunschweig, Braunschweig, Germany

Corresponding author:

Mark James Hopwood (mark@sustech.edu.cn)

Yuanyuan Gu (yuanyuan.gu1@hotmail.com)

Key Points:

- Particle tracking experiments were used to investigate the sources of high metal concentrations in the Congo Plume observed on cruise GA08
- A moderate to substantial impact of wet deposition was found, augmenting the metal concentrations at distances >1000 km from the Congo mouth
- High metal concentrations in the Congo plume are mainly from river discharge and wet deposition, with minimal influence from vertical input

Abstract

Recent work has revealed the presence of an offshore near-surface plume of dissolved trace elements in the South Atlantic Ocean (SAO). Dissolved Fe (dFe) supply from the Congo associated plume is equivalent to ~40% of the annual atmospheric dFe supply to the SAO. Yet this plume is not captured by biogeochemical models, raising questions about its exact sources. To help understand the potential source mechanisms, we use particle tracking experiments to investigate elemental distributions. Results suggest that elevated concentrations of some elements in the Congo plume are primarily sourced from river discharge and wet atmospheric deposition, with minimal influence from shelf sediments. River discharge is the main source in shelf regions and some off-shelf regions, whereas atmospheric deposition dominates the area to the southwest of the Congo River outflow. A quantitative analysis along 3°S specifically for dFe suggests a decrease in the contribution of river discharge from 90% to 30% moving off-shelf, with a corresponding increase in the importance of atmospheric deposition. Within the shelf zone, atmospheric deposition accounts for roughly 20–40%, and could be a major source of dFe around the river mouth. Integration of data from cruise GA08 reinforces the finding that wet deposition augments the concentrations of dissolved Fe, manganese (dMn) and cobalt (dCo) at distances over 1000 km from the river mouth. Given present-day patterns of nitrate, Fe, and Co limitation for primary producers in the SAO, changing rainfall patterns may have long-term implications for both regional elemental budgets and ecologically-dependent processes sensitive to trace element ratios.

Plain Language Summary

The Congo River, the world's second largest river by discharge volume, delivers substantial amounts of dissolved trace metals such as Fe (dFe) to the South Atlantic Ocean and significantly influences regional biogeochemical cycles. River, estuary and coastal surveys suggest that riverine input is the major trace metal source to the region, but this could be augmented by other sources with similar spatial distributions such as shelf sediments and rainfall. The specific contributions of these sources remain poorly constrained. Based on particle tracking simulations with neutral density parcels utilizing 'Parcels', a particle trajectories analysis framework, this work demonstrates the predominant role of Congo River discharge in trace metal enrichment within the Congo shelf zone and the importance of atmospheric deposition, particularly wet deposition in the off-shelf regions. Notably, the contribution of dFe from vertical transport processes appears negligible. Observational data obtained during 2015 further emphasize the importance of wet deposition as a source of dissolved Fe, Mn and Co in regions over 1000 km from the Congo River mouth.

1 Introduction

Micronutrients such as iron (Fe), manganese (Mn), and cobalt (Co) are essential for primary production and are often present at low concentrations in seawater such that they can (co-)limit marine productivity (Moore et al., 2013; Browning et al., 2017; Browning et al., 2021). Large areas of the ocean are termed high-nitrate, low-chlorophyll zones (HNLC) that experience Fe-limitation (Martin et al., 1990; Martin et al., 1994), largely arising from the sparse solubility of Fe in seawater (Millero, 1998). Whilst the total supply of dFe to the ocean is relatively high from mechanisms such as atmospheric deposition (Jickells et al., 2005), shelf sediments (Severmann et al., 2010) and hydrothermal vents (Yücel et al., 2011); dissolved Fe (dFe) is normally rapidly scavenged from seawater such that low nanomolar or sub-nanomolar concentrations are maintained throughout the water column. A scavenged-type element distribution is therefore typically observed for dFe in the

ocean (Missirlis et al., 2014; Hatta et al., 2015; Tonnard et al., 2020). Other scavenged-type micronutrients include Mn and Co. In contrast, elements including cadmium (Cd) and zinc (Zn) exhibit a nutrient-type distribution with depletion at the surface due to biological uptake and enhanced concentrations at depth due to remineralization (Bruland & Franks, 1983; Tagliabue, 2019; Rigby et al., 2020). River estuaries are a classic example of the inefficient delivery of scavenged-type trace elements to the ocean, especially for dFe. Whilst dFe is typically present at micromolar concentrations in river water, the salinity gradient from fresh to saline waters facilitates aggregation and flocculation of the majority of riverine dFe (Boyle et al., 1977; Sholkovitz et al., 1978). Approximately ~90–99% of riverine dFe is thought to be removed from solution in estuaries worldwide (Duinker & Nolting, 1976; Holliday & Liss, 1976; Boyle et al., 1977). For this reason, river plumes are typically not a major source of dFe to the open ocean and the associated plume-driven dFe enrichment is confined to shelf regions.

Recent work however has revealed two large-scale apparent exceptions to this generalization. Both the Transpolar Drift in the Arctic (Klunder et al., 2012; Charette et al., 2020) and the Congo River plume in the South Atlantic Ocean (SAO, Vieira et al., 2020) show nanomolar dFe enrichments that extend over ~1000 km off-shelf. The resulting dFe plumes are not captured in biogeochemical models. Models typically neglect riverine sources following the longstanding hypothesis that river plumes are localized features which do not make substantial contributions to the off-shelf marine Fe budget (Tagliabue et al., 2016). The absence of these plumes in biogeochemical models clearly indicates missing processes and thus has implications for our understanding of natural variability in regional trace metal cycling. The Congo River plume is characterized by low salinity (<25 psu) in the upper 10-m layer within the shelf region and relative high salinity (>25 psu) in the offshore region. The plume generally extends north-to- northwestwards over an area of approximately 500 km^2 (Hopkins et al., 2013; Denamiel et al., 2013) and is clearly identified in both satellite-derived chlorophyll and salinity maps (Hopkins & Polton, 2011; Hopkins et al., 2013). Regional dispersion of the plume varies significantly due to changing environmental factors, including local wind patterns, ocean circulation, and river discharge volume, resulting in notable seasonality (Signorini et al., 1999; Hopkins et al., 2013). It is estimated that the Congo plume delivers offshore dFe fluxes of $6.8 \pm 2.3 \times 10^8$ mol $year^{-1}$ to the SAO, which corresponds to 40 ± 15% of atmospheric dFe input in the region/SA/worldwide?(Vieira et al., 2020).

The strong off-shelf transport of dFe observed in these case studies raises questions about the underlying mechanism(s) and where else such effect(s) might occur. The combination of dissolved trace element distributions (Vieira et al., 2020) , Fe isotopic composition ($\delta^{56}Fe$) (Hunt et al., 2022), and radium measurements (Vieira et al., 2020) made on GEOTRACES cruise GA08 appear to corroborate that the main source of trace metals in the off-shelf plume is riverine, with minimal contribution from shelf sediments. However, Fe budgets also suggest an additional 'missing' source term that could include rainwater which overlaps spatially with the river plume (Liu et al., 2023). Whilst rainwater dFe concentrations are generally at the low end of the range observed in river water (Willey, 2000; Shelley et al., 2017), both the unique chemistry of rainwater (Kieber, 2001; Willey, 2005; Willey et al., 2008) and its rapid dilution following deposition in the ocean could make rain a more efficient dFe delivery mechanism than river water.

There are several hypotheses concerning why some rivers may more efficiently deliver dFe to the off-shelf ocean compared to others. Organic ligands are an important feature of the Fe cycle and ligand-bound Fe is the major component of dFe in seawater, accounting for ~99% of dissolved Fe(III) (Gledhill & Buck, 2012), with inorganic species minor in comparison. Whilst river water

is enriched in both organic ligand and dFe concentrations compared to the ocean (Powell & Wilson-Finelli, 2003; Su et al., 2015), ligands are also subject to estuarine removal (Sholkovitz et al., 1978). Yet some types and size-fractions of organic material may be less susceptible to estuarine removal processes than others (Gustafsson et al., 2000; Krachler et al., 2005). The Congo River and the Siberian shelf regions which feed the Transpolar Drift both feature extensive peat deposits. These deposits may be associated with organic material that is less prone to estuarine removal and thus potentially facilitates a more efficient land-to-ocean transfer of dFe (Krachler et al., 2010). A heavy δ^{56}Fe signal of dFe in the Congo plume could be consistent with a role of strong ligands in preserving the high dFe concentrations present (Hunt et al., 2022).

An alternative hypothesis is that the effect is largely physical. Major river outflows are typically constrained along the shelf by a combination of buoyancy and rotational effects, as is the case for the Amazon River (Coles et al., 2013) and the Mississippi River(Walker et al., 2005). The Congo River outflow is particularly unusual as it is the only major river system worldwide to produce a plume in an eastern boundary region close to the equator. A combination of fast ocean currents and weak Coriolis acceleration could thereby advect material from the Congo outflow off-shelf more efficiently than would be the case if the river were present at higher latitudes. Here, in order to study the underlying mechanisms maintaining the Congo-derived dFe plume in the SAO, we conduct a suite of particle tracking experiments. Particle tracking experiments release an inert tracer into a regional model. Here they are used to investigate the physical dynamics of the Congo-derived plume in the absence of confounding chemical effects in order to de-couple chemical and physical mechanisms.

2 Materials and Methods

2.1 Study region

The study area extends from 0°–20°S and from 2°W–14°E. The Congo River flows into the ocean at 6°S, 12.3°E, with the Congo River plume primarily concentrated north of 10°S. In this work, the Congo shelf is defined as the region within 500 km of the Congo River mouth, while the off-shelf region refers to areas beyond 500 km (Figure 1). More detailed information about the physical environment can be found in previous descriptive studies (Hopkins et al., 2013; Hunt et al., 2022).

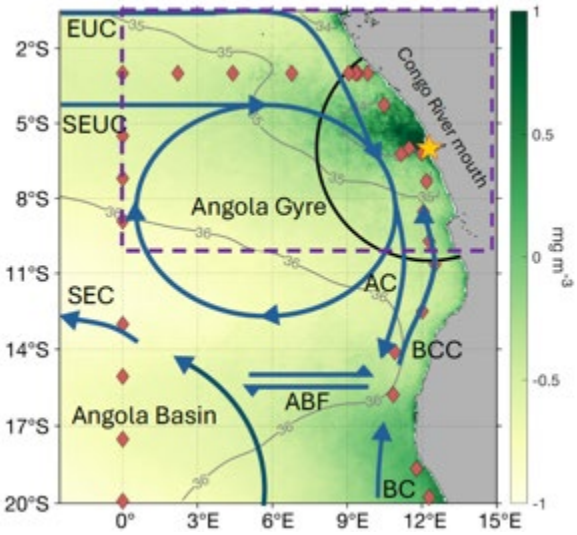

Figure 1. Map of study region with surface and subsurface circulation patterns overlain: Equatorial Undercurrent (EUC), South Equatorial Undercurrent (SEUC), Angola Current (AC), Benguela Current (BC), Benguela Coastal Current (BCC), and South Equatorial Current (SEC). The Angola-Benguela Front (ABF) is formed by the northward-flowing BC and the southward-flowing AC. The cyclonic Angola Gyre, centered at (10°S, 5°E), is formed by the AC. The orange star marks the Congo River mouth. The background shows the climatological chlorophyll distribution (in mg/m3), with rhombic markers indicating GA08 stations. The purple box highlights the Congo Plume region and the solid black curve delineates the boundary between the shelf and off-shelf regions.

2.2 Dissolved Fe input calculation

The sources considered in our particle tracking experiment are atmospheric deposition (wet and dry deposition), riverine discharge, and the upward vertical flux of dFe to the surface-ocean layer. The vertical flux incorporates sources that would require vertical transport to be present in the near-surface Congo plume, e.g., submarine groundwater and shelf sedimentary inputs. In the following sections, we describe how the gridded dFe inputs were estimated. For consistency, gridded dFe fluxes were interpolated to a resolution of 0.25° × 0.25°. Here, the profile samples collected on R/V Meteor cruise M121 (GEOTRACES GA08) (Frank et al., 2016) during the period 22 November to 27 December 2015 were used to calculate the vertical dFe flux. A comprehensive description of the data and GEOTRACES quality control procedures are available in prior work (Vieira et al., 2020; Liu et al., 2022a; Liu et al., 2023). Additionally, to validate our simulations, profiles of other trace metals measured during the cruise, including dCo, dMn, dCu, dZn dCd, dNi, and dPb, are also analyzed.

2.2.1 Vertical dFe flux

Temperature, salinity, O_2, and dFe profiles collected during GA08 were used to calculate the vertical dFe flux at each station and estimate the distribution of vertical dFe fluxes over the study region. The vertical dFe flux (μmol m^{-2} d^{-1}) to the mixed layer (ML) associated with diapycnal mixing and upwelling velocity is expressed as (Steinfeldt et al., 2015; Tanhua & Liu, 2015):

$$Flux = k_z \frac{dFe}{dz} + w(C_2 - C_1), \quad (1)$$

where the first term in equation (1) is the diffusive dFe flux and the second term is the flux associated with vertical transport.

Parameter k_z in the first term is the turbulent diffusivity coefficient (m^2 s^{-1}), which was assumed to be 10^{-4} m^2 s^{-1} (Liu et al., 2022a). This value is consistent with observed k_z=1.0–1.7 ×10^{-4} m^2 s^{-1} below the mixed layer at ~40°S in the South Atlantic (Hsieh et al., 2021) and an estimated k_z range of 10^{-6} to 10^{-4} m^2 s^{-1} in other ocean basins (Ledwell et al., 1993; Martin et al., 2010; Dunckley et al., 2012; Tanhua & Liu, 2015). The ML depth was calculated as the interpolated depth at which the potential density difference from 10 m depth was 0.03 kg m^{-3} (de Boyer Montégut, 2004). The dFe concentration gradient dFe/dz (mol L^{-1} m^{-1}) was calculated by linearly fitting the dFe concentration-depth relation for all measurements from the ML (average dFe concentration in the ML) to 100 m below the base of the ML.

In the second term of equation (1), wind-driven upwelling velocity (w, m s^{-1}) due to offshore Ekman transport (Ekman coastal velocity, w_e) and wind stress curl (Ekman pumping, w_c) were calculated as follows (Bordbar et al., 2021):

$$w_e = \frac{2.07 \times T}{R} e^{2.3026(-x/R)}, \quad (2)$$

$$w_c = curl\ (\tau)/(\rho_w f), \quad (3)$$

where R is the first baroclinic Rossby radius of deformation (km). The 1° ×1° global gridded R (Chelton et al., 1998) was obtained from https://ceoas.oregonstate.edu/rossby_radius (last accessed in May 2023). T is the offshore Ekman transport ($m^2\ s^{-1}$), x is the distance to the coastline (km), f is the Coriolis parameter (s^{-1}), ρ_w=1025 kg m^{-3} is the mean density of the upper-ocean layer, and $curl\ (\tau)$ is the wind stress curl (Pa m^{-1}). Wind stress τ (kg $m^{-1}\ s^{-2}$) is expressed as

$$\tau = \rho_a C_D U_c |U|, \quad (4)$$

where the drag coefficient C_D and air density ρ_a were assumed to be 1.12×10^{-3} and 1.25 kg m^{-3}, respectively. U is the wind speed magnitude at 10-m height and U_c is the zonal or meridional wind speed. Daily wind speed data with a resolution of 0.25° from 2013 to 2022 was obtained from the European Centre for Medium-Range Weather Forecasts (ECMWF) fifth-generation ERA5 reanalysis product (Hersbach et al., 2023). The climatological daily wind speed was calculated and used to estimate the gridded vertical dFe flux across the study region. For all stations, wind speed was extracted from the averaged wind field during the GA08 cruise period in 2015 to calculate the corresponding vertical dFe flux (Figures 2b and 2c).

The eastward and northward Ekman transport T_x and T_y can be derived according to the zonal and meridional wind stress τ_x and τ_y, respectively:

$$T_x = \frac{\tau_y}{\rho_w f} \text{ and } T_y = -\frac{\tau_x}{\rho_w f}. \quad (5)$$

To simplify the calculation of the offshore Ekman transport driven by alongshore winds, we assumed the coastline angles — defined as the angles between true west (0°) and the coastline, measured clockwise — to be 62°, 108°, and 69° for the regions 0°–11°S, 11°–17°S, and 17°–20°S, respectively. In addition, in the coastal region within R, the sum of w_e and w_c was applied to estimate the vertical flux, while for the region beyond R, upwelling velocity associated with offshore Ekman transport (w_e) was neglected.

The average dFe concentration (nmol L^{-1}) in the ML is represented by C_1, and C_2 is the dFe concentration 20 m below the base of ML. Because of the sparse spatial resolution of the profile observations, C_2 was estimated according to the dFe concentration gradient (i.e., dFe/dz), thereby the term $(C_2 - C_1)$ was calculated as

$$C_2 - C_1 = 20 \times dFe/dz. \quad (6)$$

Considering the importance of dissolved O_2 in controlling dFe concentration in the water column, especially in shelf environments with pronounced O_2 minima and associated plumes of redox-sensitive elements (Hong & Kester, 1986; Noble et al., 2012; Rapp et al., 2019), we assessed the relationship between dO_2/dz and dFe/dz based on all cruise observations and found a reasonable linear fit (dFe/dz = -0.0143 dO_2/dz - 0.0213, Figure 2a). This relationship was used to estimate the regional gridded dFe vertical flux. The method estimating dO_2/dz was the same as per dFe/dz

above. Gridded observation-based monthly climatological dissolved oxygen data was derived from World Ocean Atlas 2018 (WOA18), with a resolution of 1° × 1°. Since high-temporal-resolution dissolved oxygen data are currently unavailable, we resample the monthly WOA18 data for specific months to obtain the daily oxygen concentrations. Based on this dO_2 data, we are able to estimate the daily gridded dFe/dz. Therefore, the observed vertical dFe flux for 48 GA08 stations can estimated based on measurements and equations (Equation (1)–(6)), and the gridded vertical dFe flux during the cruise period and the climatological daily vertical dFe flux for the entire study area can be estimated using the equations above, along with the gridded data and constructed dO_2/dz and dFe/dz relationships. Overall, the observed vertical dFe flux aligned reasonably well with our estimated values (Figure 2b), despite the use of different time windows imposed by data availability limitations. It is important to note that this is only a rough comparison to assess the relative importance of different source terms, a detailed estimation of vertical dFe flux and its components for each station is out of the scope of this study. The climatological daily gridded vertical dFe is primarily used in the following analysis.

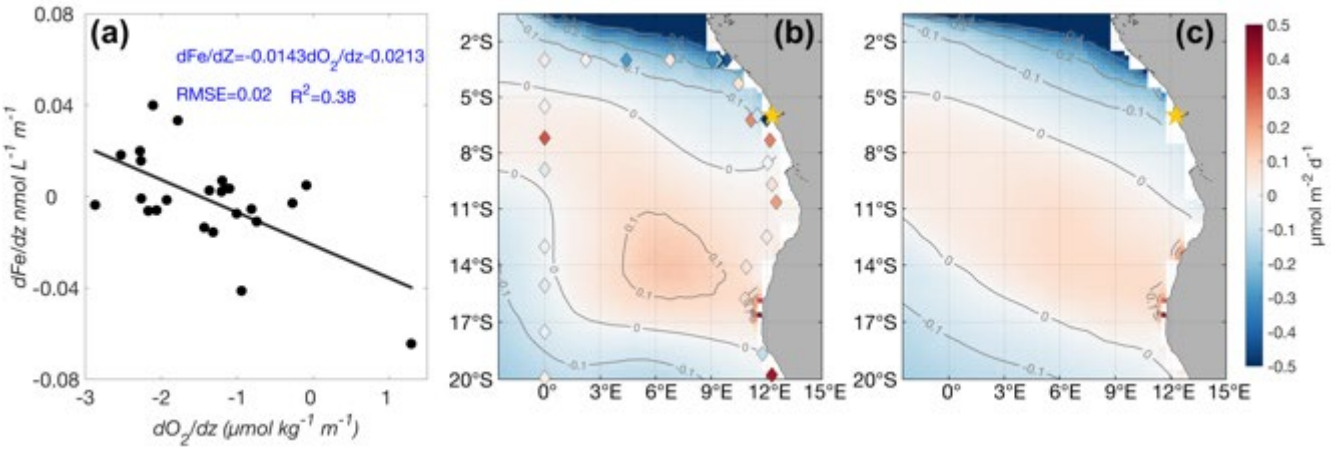

Figure 2. Estimating vertical Fe fluxes (μmol m^2 d^{-1}) based on dFe and dO_2 distributions over the Congo region. (a) Changes in dFe/dz with dO_2/dz over the Congo region. Black cricles are from measurements; linear fit is shown as a solid black line. (b) Map of estimated dFe vertical flux during the cruise period is projected using the equation shown in (a), where rhombic points represent the observed dFe fluxes from GA08 stations. (c) Map of projected climatological vertical dFe flux. In (b) and (c), the orange star marks the Congo River mouth.

2.2.2 Atmospheric dFe input

Atmospheric deposition of dFe (F, μmol m^{-2} d^{-1}) is often estimated as the sum of dry and wet deposition though with some differences concerning what processes are captured between studies (Schulz et al., 2012). Monthly deposition rate of dust (kg m^{-2} s^{-1}) at 1° resolution during the period of 2001/01 to 2014/12 was obtained from the GISS-E2-1-G Earth System Model. The GISS-E2-1-G model was chosen because it captures the spatial distribution of dissolved aluminum concentrations, used as a tracer of dust deposition (Measures & Brown, 1996), and is referred to as a best-fitting optimized model (Xu & Weber, 2021). The period from 2001 to 2014 was selected to calculate the climatology because dust data is not available after 2014. To estimate dFe input via dry deposition (F_{dry}, μmol m^{-2} d^{-1}), we assume Fe fractional solubility is 2% (Guieu et al., 2005; Theodosi et al., 2010), and assume an Fe abundance in dust of 5.04%, as per upper continental

crust (Rudnick & Gao, 2014). Monthly data was interpolated into daily dust dFe input for the following analysis.

Satellite observations of daily accumulated precipitation (p, mm d^{-1}) from 2001/1/1 to 2014/12/31 were obtained from NASA's Global Precipitation Measurement (GPM) mission. The measured volume-weighted-mean dFe concentration in rainwater within the Congo shelf (~3°–8°S, ~9°–12.5°E) during GEOTRACES cruise GA08 was c_{wet} = 11.3 nmol L^{-1} (Liu et al., 2023). This concentration was also applied to off-shelf areas due to data deficiency. The wet deposition of dFe (F_{wet}, μmol m^{-2} d^{-1}) was estimated as:

$$F_{wet} = p \times c_{wet}. \quad (7)$$

Accordingly, the average distribution of total atmospheric dFe deposition (dry + wet), dry, and wet deposition were computed (Figure 3). The considerably weaker magnitude of the average dFe flux from dry deposition compared to the wet deposition flux indicates the dominant regional role of wet deposition. This was especially the case in the region influenced by the Congo plume (Figure 3).

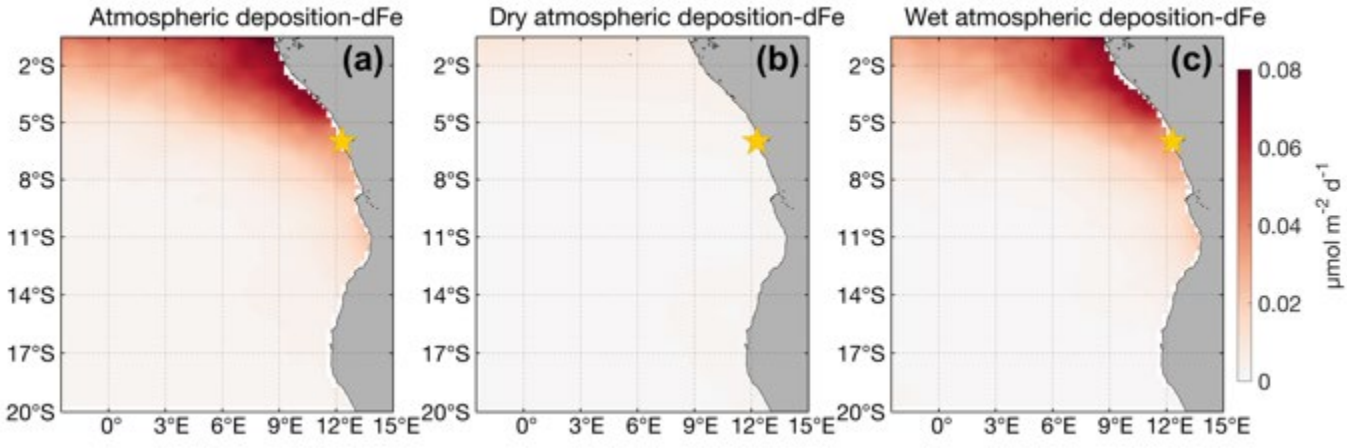

Figure 3. Average distribution of atmospheric dFe deposition flux (μmol m^2 d^{-1}): (a) dFe input flux via total atmospheric deposition (wet + dry); (b) dry deposition flux of dFe; and (c) wet deposition flux of dFe. The orange star marks the Congo River mouth.

2.2.3 Riverine dFe discharge

Daily river discharge (m^3 s^{-1}) observations at station Kinshasa was obtained from the Global Runoff Data Centre (GRDC). The period from 2001 to 2010 was selected to calculate the climatological daily river discharge volume because the data is not available after 2010. Kinshasa is 500 km upstream of the Congo River mouth. Assuming an average downstream flow speed of 0.1 m s^{-1}, the discharge signal to the Congo River mouth is delayed by roughly 1.5 months (Hopkins et al., 2013; Martins & Stammer, 2022). A climatological monthly time series of dFe concentrations was available in the estuary at intermediate salinities (Araujo et al., 2014). This dataset compiled the discharge of dFe concentrations from the Congo river, sourced from multiple discrete surveys conducted between 1978 and 2009, and then applied an 80% loss rate due to low-salinity flocculation to reflect the monthly net input of riverine dFe concentrations to the ocean.

Whilst non-conservative removal of dFe is not instantaneous (Mayer, 1982) such that any flux derived at intermediate salinities will be defined at a point of intermediate removal, estuarine dFe distributions—almost invariably—indicate the most rapid removal of dFe at low salinities (0–10 psu) (Boyle et al., 1977). The available estuarine time series at salinities ~7.5–12.5 psu (Araujo et al., 2014) therefore likely captures the majority of removal and is more useful for modeling the offshore propagation of dFe than measurements of freshwater concentrations which have yet to be mixed in the estuary.

To estimate dFe inputs, we multiplied the climatological daily river dFe concentration (nmol L^{-1}) in the estuary (Araujo et al., 2014) with daily river discharge volume (m^3 s^{-1}) to calculate the year-round daily dFe mass discharge rate (mol d^{-1}) from the Congo River (Figure 4). The dFe flux (µmol m^{-2} d^{-1}) to the river plume was estimated with the assumption that the freshwater plume area is 5 $\times 10^5$ km^2 (Hopkins et al., 2013).

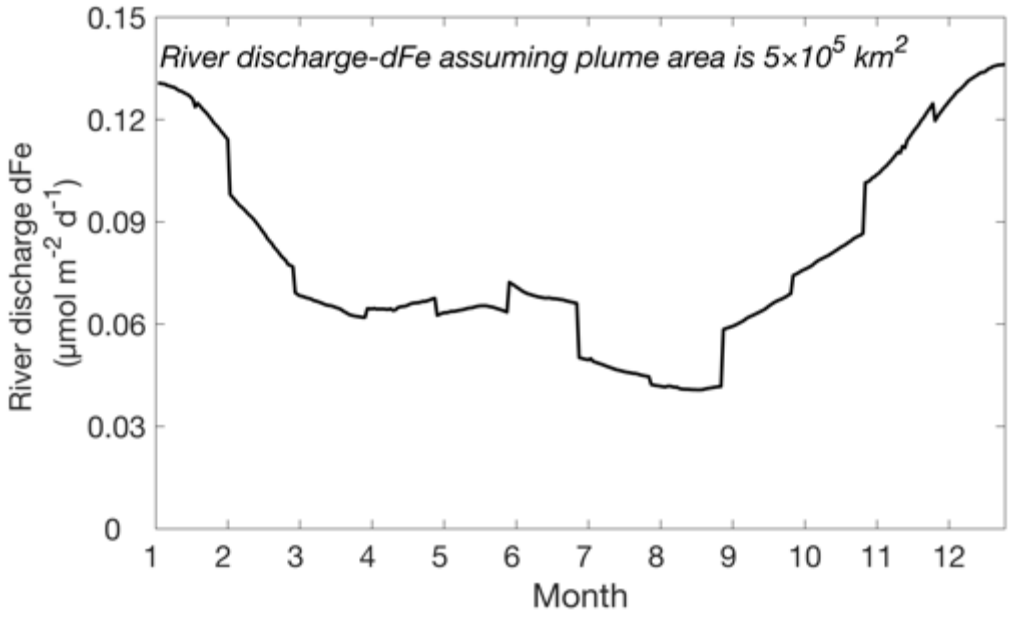

Figure 4. Time series of average monthly dFe input (µmol m^2 d^{-1}) from Congo River discharge. Month 1 equals… (January 2015?)...

2.3 Particle tracking experiment

To quantify the spatial dispersion of dFe from Congo River discharge, atmospheric deposition and vertical transport, particle tracking experiments were conducted using OceanParcels (Probably A really Computationally Efficient Lagrangian Simulator, http://oceanparcels.org), a novel offline Lagrangian tracking model advecting particles and simulating particle trajectories using a fourth-order Runge-Kutata scheme (Lange & van Sebille, 2017; Delandmeter & van Sebille, 2019). OceanParcels is accurate in idealized and realistic simulations (Delandmeter & van Sebille, 2019; Eddebbar et al., 2021), and is commonly used in recent pathway studies due to its scalable computation and flexible coding rule (Capó & McWilliams, 2022; Seijo-Ellis et al., 2023; Youngs et al., 2023; Carlson et al., 2024). We use daily-mean surface-ocean currents during 2015 from the GLORYS12 (*GLORYS12V1*) product, an eddy-resolving reanalysis with a 1/12° horizontal resolution as the input flow field. We use the 2015 ocean current data instead of the climatological

current fields to advect the particles because ocean currents are crucial drivers in determining the transport of dFe in the Congo region. Using time-mean current field would average out important meso- and sub-mesoscale processes. Additionally, previous studies have provided observational evidence of dFe enhancement in the Congo Plume region during 2015, with interannual variability yet to be constrained, so utilizing the 2015 current data to drive the simulation could help elucidate the potential mechanisms. Therefore, the study is based on the assumption that dFe concentration and input do not exhibit significant interannual variability and that the plume of dFe associated with the Congo outflow into the SAO is a recurring feature — which is yet to be explicitly shown. In the experiment, particles that ended up getting stuck on land were removed during the experiments for simplicity.

Three sets of experiments were conducted where we tracked particles. In all three experiments, we ran OceanParcels for one year (January 1, 2015 to December 31, 2015), and also for half a year (January 1, 2015 to June 30, 2015). Because particles were advected using the same method, the trajectories remain unchanged if the particles were released from the same day/location and tracked during the same period. In order to reflect the real dispersal of dFe in the ocean, we scaled 1 particle to represent 1 mol dFe. In the 'Congo River input simulation' experiment, particles were released at daily intervals in the surface layer of the Congo River mouth (12.3°E, 6°S) from January 1, 2015. To simulate the dFe input in the real ocean, the count of particle trajectories in each grid cell was multiplied by the long-term mean riverine dFe mass discharge per day measured in mol d^{-1}, the result is named as the 'trajectory density'. The trajectory density reflects the probability of a particle appearing in a specific grid. The higher the density, the more likely it is for a particle to be found in that grid. Similarly, to track the dFe dispersal sourced from atmospheric deposition in the 'atmospheric deposition input simulation', particles were released at each grid cell in the study region at daily intervals (Figure 3) and their trajectories were also tracked for 2015. We then estimated the trajectories density for each grid cell according to the particle trajectories and dFe amount (mol d^{-1}) calculated from grid area (m^2) and time-mean gridded dFe flux (mol m^{-2} d^{-1}). In the 'vertical input simulation', particles sourced from vertical transport were similarly scaled based on the average upwelled dFe flux (mol m^{-2} d^{-1}). In this case, particles were only released at grid locations when the gridded vertical dFe flux was positive in order to maintain comparability with the atmospheric and river experiments which represent gross fluxes and do not remove particles to simulate dFe sinks.

3 Results

3.1 Simulated dispersal of dFe in the Congo plume

Our primary investigation focuses on the dispersal patterns and their short-term (below annual timescales) variations in the region north of 10°S. Simulations depicting the dispersal of dFe from the Congo River reveal that the highest trajectory density occurs along the coast from 6°S to 3°S, particularly over the inner shelf close to the release location. Three hotspot regions were formed: 1) large amounts of particles extended northwestward into the open ocean after departing from the coastline; 2) some particles dispersed westward at approximately 3°S; and 3) a portion of particles flowed in a southwestern direction (Figure 5a). Dispersal patterns corresponded with the year-round spatial patterns of Chl-a and low-salinity dynamics as detected from satellite observations (Hopkins et al., 2013). The comparison shows that dispersal generally follows the plume of the northwestward extension along the coastline between November and February, a westward to

south-westward extension from February to April/May, and a westward extension from June to August.

For river discharge, there was good consistency in the distribution of frequencies between the 1/2 year and 1 year simulations (Figures 5a and d). This consistency arises from the accumulated trajectories between January and June, and southward and northward transport of the majority of particles along the coastline during the latter half of the year 2015 (Figure S1) driven by ocean currents. The seasonal variability of the currents reveals that a northward-to-northwestward flow advecting particles from the Congo River begins to emerge in February. This flow strengthens until June and starts to decay in July. In September, an opposing eastward-to- southeastward current develops and intensifies, leading to southward transport of the particles sourced from Congo River (Figure S2). In contrast to the particles from river discharge, atmospheric deposition tracers were more sensitive to seasonal differences (Figures 5b and 5e). Higher trajectory densities from atmospheric deposition were observed in the southeast (Liu et al., 2023). For the 1 year simulation, the dispersal pattern was similar to the 1/2 year simulation but the atmospheric trajectory frequencies increased over the whole region (Figure 5e and 5b). For both 1 year and 1/2 year simulations, particles associated with vertical transport (Figure 5c and 5f) demonstrated limited dispersal north of ~6°S because of the negative or weak dFe vertical flux prevailing in this region. In contrast, notably enhanced frequencies were found within the Angola Gyre, identified as an upwelling zone (Gordon & Bosley, 1991; Signorini et al., 1999). A lower k_z=1 x 10^{-5} m^2 s^{-1} was also applied in the vertical transport calculation to test the impact of k_z on the dFe vertical flux. This resulted in even weaker upwelled dFe flux but maintained a similar distribution in the study region (Figure S3). Therefore, subsequent analysis focuses only on contrasting trajectory frequencies resulting from river discharge and atmospheric deposition inputs.

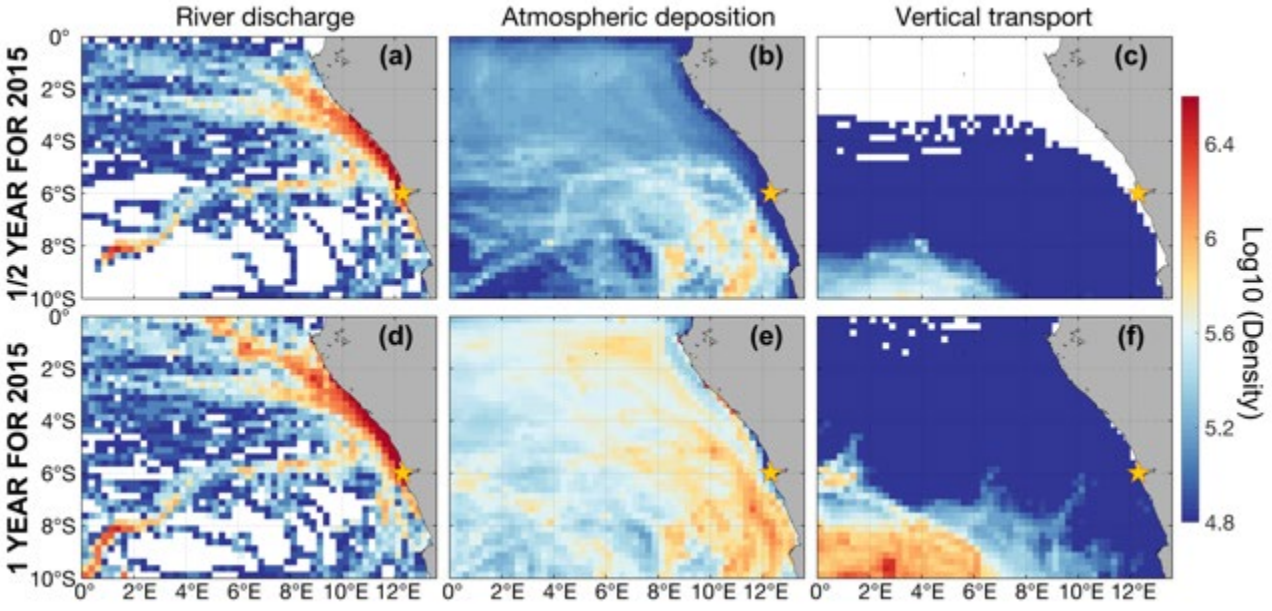

Figure 5. Distribution of trajectory density for particles sourced from river discharge, atmospheric deposition, and vertical transport scaled to represent gross dFe fluxes. (a) and (d) show river discharge sources, (b) and (e) show atmospheric disposition sources, and (c) and (f) show vertical transport sources. (a)–(c) are 1/2 year simulations from January to June 2015 and (d)–(f) are 1 year simulations during 2015. The orange star marks the Congo River mouth.

3.2 Trace metals sources to the Congo plume along the GA08 transect

A comparative analysis was conducted by calculating the ratio of trajectory frequencies attributed to river discharge input relative to the combined frequencies stemming from atmospheric deposition and river discharge for the GA08 cruise transect. This calculation serves to quantify the relative influence or strength of the two distinct sources under consideration. For instance, a ratio of 0.5 signifies an equivalent contribution from riverine and atmospheric sources, whereas a ratio >0.5 indicates dominant influence from the riverine source and a ratio <0.5 indicates the dominant role of atmospheric deposition. For the 1/2 year simulations, the dispersal in the shelf region (<500 km from the Congo River mouth) and patchy off-shelf region (>500 km from the Congo River mouth) mainly north of 3°S was primarily due to riverine sources. Conversely, in the southwest of the plume region and part of the open ocean north of 3°S, atmospheric deposition emerges as the predominant source of dFe. Similar distributions also emerged in the context of the 1-year simulation scenario, albeit with the riverine- dominant region exhibiting a reduced offshore extension and a spatial distribution more constrained to the coast (Figure 6a and 6b).

The high-resolution near-surface station and towfish observations obtained during cruise GA08 (Figure 6a) provided an opportunity to quantitatively validate simulated dFe sources within the plume region. A multi-element comparison is also informative although the relative importance of riverine and atmospheric sources likely varies between elements. To integrate the simulated dFe sources with observations, we first calculated the contributions originating from river discharge and atmospheric deposition based on trajectory frequencies at the sampling points of the GA08 transects (Figure 6c and 6d). In both 1 year and 1/2 year simulations, there were notable shifts in the contributions of dFe sources along the GA08 transects. As distance increased from 9°E to the further off-shelf region, the computed proportion of dFe sourced from river discharge decreased substantially from approximately 90% to 30%. The contribution from atmospheric deposition showed a corresponding rise, increasing from about 10% to 70%. These changes were particularly pronounced between the longitudes of 9°E and 3°E. Specifically, in the 1/2 year simulation, the dominance of river discharge was more pronounced to the east of 4.5°E and less to the west of 4.5°E due to the wet atmospheric deposition source (Figure 6c). As the simulation duration increased, the region where atmospheric deposition was dominant expanded eastward, such that it surpassed the contribution from river discharge at all stations west of 7°E (Figure 6d). However, in the Congo shelf zone, both atmospheric deposition and river discharge inputs played significant roles, depending on the specific location.

For shelf observations west of 11°E (or north of 5°S) close to the eastern-most station of the 3°S transect, the dominant influence of river discharge was evident, contributing over 50% of dFe. Meanwhile, significant contributions of dFe from atmospheric deposition were sporadic, reflecting the patchy nature of wet deposition, particularly near the Congo River mouth (south of 5°S or east of 11°E), where contributions as high as 90% from atmospheric deposition occurred. On average, estimated contributions from atmospheric deposition over the Congo shelf region were roughly 20% and 40% for 1/2 year and 1 year simulations, respectively. Therefore, the 3°S transect, extending from Congo shelf to the open ocean, was subsequently categorized as a river dominant zone to the east of 7°E and an atmospheric deposition dominant zone west of 4.5°E. Given the considerable uncertainty in the measurement of dFe concentration in rainwater (11.3 ± 4.9 nM), a sensitive analysis was conducted using a lower bound (~6.4 nM) and an upper bound (~16.2 nM) based on the standard deviation of the measured dFe concentrations. Although the density magnitude differs from that derived using the average dFe concentration (Figure S4), the results

indicate that wet deposition plays a significant role in the Congo Plume region, relative to river discharge (Figures S5 and S6).

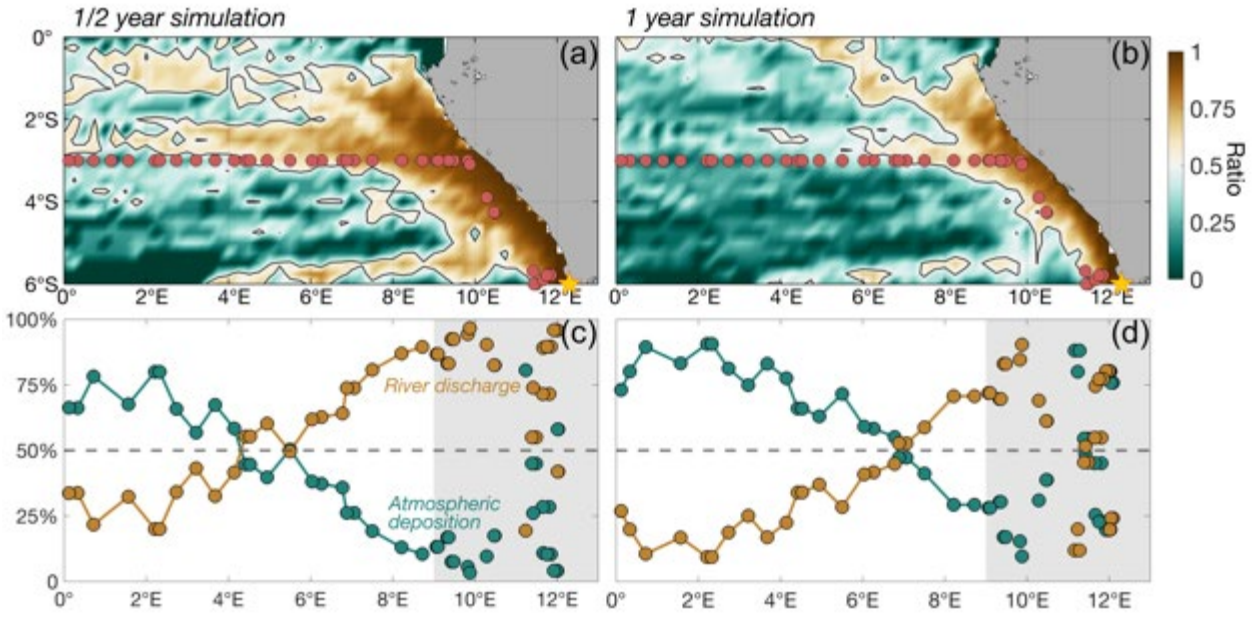

Figure 6. The contribution of river discharge and atmospheric deposition to dFe input in the Congo plume. (a) and (b) show the density ratio of river discharge to the sum of input from river discharge and atmospheric deposition; white contours indicate a ratio of 0.5 (i.e., equivalence between riverine and atmospheric sources). Red dots represent locations of towfish and station samples at depths <35 m along 3°S and in the shelf zone from cruise GA08. (c) and (d) show the contribution of river discharge (orange circles) and atmospheric deposition (green circles) changing with longitude along GA08 transects, with the shelf region shaded in grey. (a) and (c) show the contributions from 1/2 year simulations; (b) and (d) show the contributions from 1 year simulations. The orange star marks the Congo River mouth.

In the river-dominant zone, salinity levels generally exhibit lower values (ranging from 33.0 to 35.2 psu) compared to that in the atmospheric deposition-dominant zone, where salinity ranged from 34.7–35.8 psu. Theoretical conservative mixing curves were constructed for dFe and seven other trace metals along 3°S for all samples (Figure 7, grey dotted lines), as well as for samples specifically within the river-dominant zone (Figure 7, black dotted lines). Within the river-dominant zone, all elements except dPb exhibited a linear decrease with increasing salinity offshore, suggesting that freshwater is a major source for these elements. However, it's noteworthy that the dMn and dZn trends were not statistically significant (P value > 0.05). When incorporating observations from the atmospheric-deposition-dominant zone (Figure 7, grey lines), the gradients of the theoretical conservative mixing curves of all elements are reduced compared to those derived solely from observations in the river-dominant zone. This discrepancy corroborates the distinct spatial boundaries defined by the particle tracking experiments and suggests variations in the observed trace metal sources between these two zones.

It should be noted however that only three processes are considered herein (atmospheric deposition, discharge from the Congo River, and vertical transport). The Congo River is by far the largest river by discharge in the region of interest, but freshwater input from the Ogooue and

Kouilou-Niari Rivers might also contribute to metal distributions. Herein we have referred to the prominent offshore extension of the low-salinity plume from the coast to 0° in the region north of the Congo River mouth as the 'Congo plume' (Figure S7), following the method of Hopkins et al. (2013) (Figure S8). Yet particularly during the high river discharge seasons, i.e., from November to May (Mignard et al., 2017; Laraque et al., 2020) the plume is not necessarily derived exclusively from Congo discharge. Additionally, when extrapolating the results from dFe particle experiments to other elements, the different ratios of these elements in rain and river water should be considered. For simplicity, we have run particle tracking experiments and defined atmospheric/riverine zones of influence based on dFe budgets. However, the riverine and atmospheric dominant zones could exhibit disparities for other elements owing to variations in their respective inputs. Thus, we also compared riverine input (C_{river}) with element concentrations from wet deposition in the Congo shelf (C_{wet}) to briefly discuss to what extent the behavior of other trace metals may follow, or diverge from dFe. The ratio of C_{wet} / C_{river} for Cd, Co, Mn, and Ni, ranging from 2.3–3.3, were found to be of comparable magnitude to that of Fe (1.0), implying that the dominant zones for these elements would be approximately consistent with dFe. However, C_{wet} / C_{river} ratios were 20–430 times higher for Cu (20), Pb (266), and Zn (430) compared to those for dFe (Figure S9 and Table S1). If all other factors remained constant, this discrepancy would indicate that the dominant zones of riverine and atmospheric deposition for these elements would be different from dFe, and in all cases the river-dominant zone would be more constrained in the shelf region. However, there are certainly other associated uncertainties from the assumptions used to design the particle tracking experiment for dFe, namely the varying solubility of different elements in atmospheric deposition and the varying significance of vertical fluxes.

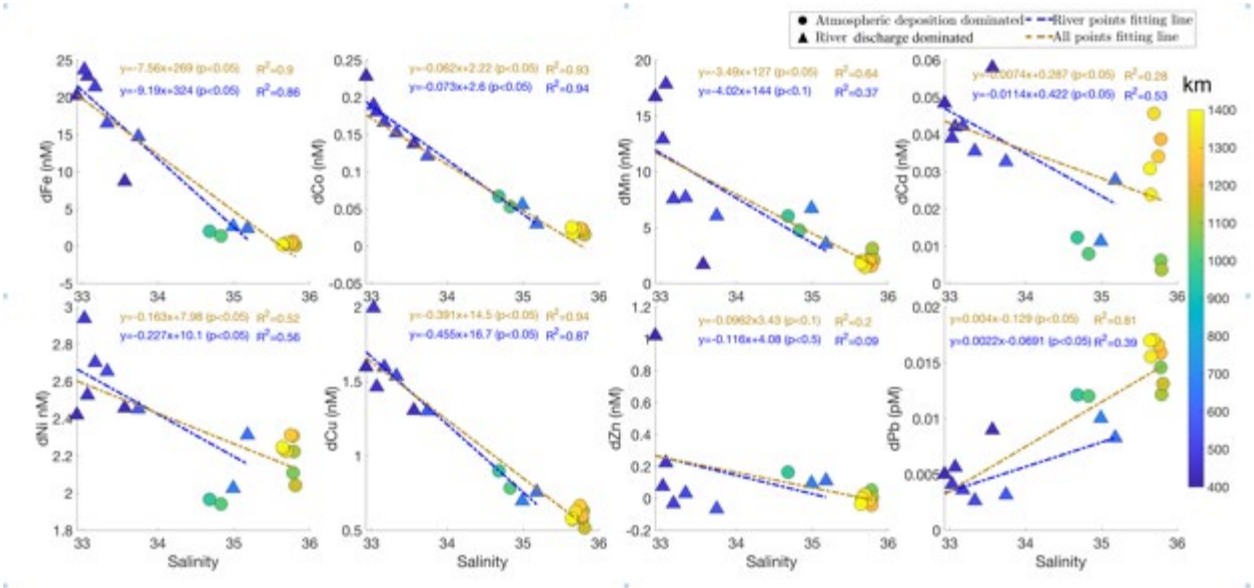

Figure 7. Surface-ocean dissolved trace metals concentration (<10 m) with increasing salinity. Data is separated into zones where the dFe budget was dominated by riverine (triangles) and atmospheric deposition (circles) sources along 3°S. The marker color represents the distance between the Congo River mouth and sampling locations. Dotted lines represent the linear fit for all observations (grey line) and observations in riverine-dominant zone (black line).

From the relationships between elemental concentrations and distance from river mouth to sampling locations, a declining trend in the concentrations of all trace elements, except dPb, was

observed with increasing distance within the river-dominant zone (Figure 8). This relationship further supports the notion that river discharge served as the primary source contributing to the plume in this zone within a proximity of 800 km from the Congo River mouth. Notably, elevated concentrations of dFe, dCo, dMn, dCu, and dZn with a ratio <0.5 (i.e., atmospheric deposition dominance) were observed at a distance of roughly 1000 km from the river mouth within the atmospheric dominant zone. With limited influence from river discharge in this zone, the variability of the distribution of the ratio (Figure 8, see colors) may be linked to local precipitation events. Yet uncertainties in off-shelf rainwater dFe concentrations, and the changing significance of other sources, including those not considered herein for dFe (e.g., vertical fluxes and dry deposition) should also be noted. Moving further offshore, anomalous increasing trends were observed for dCd, dNi, and dPb beyond 1000 km from the Congo River mouth indicating differences in the source mechanisms compared to the assumptions used to trace dFe.

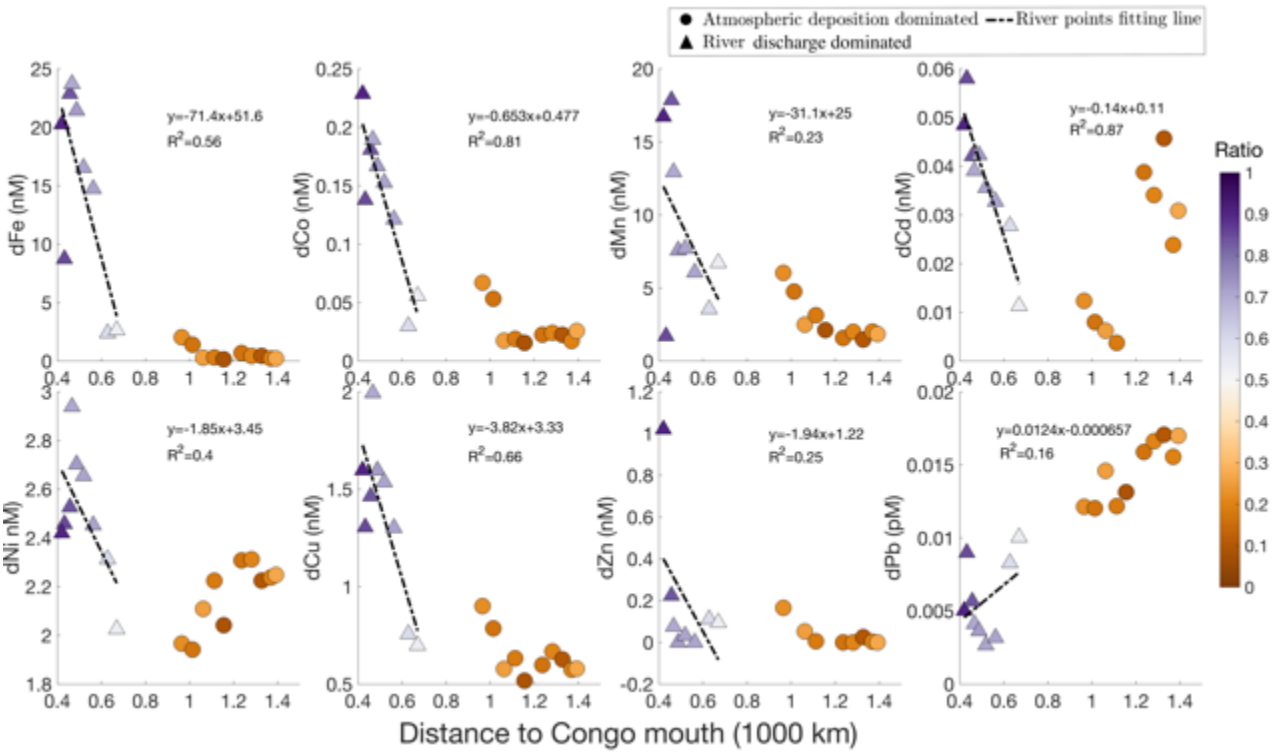

Figure 8. Surface-ocean dissolved trace metal concentrations (<10 m) with increasing distance from the Congo River mouth. Data is separated into zones where dFe supply was dominated by riverine (triangles) and atmospheric deposition (circles) sources along 3°S. Marker color represents the density ratio of river discharge to the sum of input from river discharge and atmospheric deposition for dFe at each sampling location to indicate a river discharge dominated zone (>0.5) and an atmospheric deposition dominated zone (<0.5). Dotted lines represent the linear fit for observations (in black) in the river-dominant zone.

3.3 Impact of seasonality on dFe sources in the Congo plume

The significant seasonal cycle of river discharge results in the highest average input of dFe in December, approximately $6.5 \cdot 10^{10}$ µmol d^{-1}, and the lowest input in August of roughly $2.1 \cdot 10^{10}$ µmol d^{-1}(Figure 4). Concurrently, due to seasonal fluctuations in precipitation, the annual average dFe input from atmospheric deposition in the Congo plume region peaks in March and reaches its

minimum value in July. The lowest monthly deposition flux is 44 times lower than the peak value. Given the notable seasonal variability of salinity and chlorophyll-a (Chl-a) in the Congo plume region, which are influenced by oceanic environmental factors such as wind speed, precipitation, ocean currents, and river discharge (Signorini et al., 1999; Hopkins et al., 2013; Martins & Stammer, 2022), it is likely that the drivers of dFe and other trace element distributions in the Congo plume are also subject to significant seasonal variability. To evaluate the sensitivity of the mechanisms that maintain dFe in the Congo plume to seasonal variability in dFe inputs, particle dispersal under four extreme scenarios is presented. These scenarios represent maximum and minimum dFe input from monthly average river discharge combined with annual average distribution of dFe input from atmospheric deposition (Figures 8a–8d), and maximum and minimum atmospheric deposition field combined with annual mean riverine input (Figures 8e–8h). Similar to the scenarios using mean inputs, under the conditions of maximum river input, mean atmospheric input (Figure 9a and 9b); minimum river input, mean atmospheric input (Figure 9c and 9d); and mean river input, maximum atmospheric input (Figure 9e and 9f), dFe sources in the Congo plume are predominantly attributed to atmospheric deposition in off-shelf regions spanning from 0° to 3°–7°E and 6°–8°E for 1/2 year and 1 year simulations, respectively. In contrast, in other off-shelf zone <9°E, riverine dFe dominates. Additionally, within the Congo shelf zone, river discharge remains the main source to the west of 11°E (or north of 5°S), while both river discharge and atmospheric deposition play significant roles in regions near the river mouth (Figures 8a–8f). When dFe input from atmospheric deposition is set to minimum values, the Congo plume region is entirely dominated by the river discharge as expected, with contributions exceeding 80% for the 1/2 year simulation and 60% for the 1 year simulation (Figures 8g and 8h).

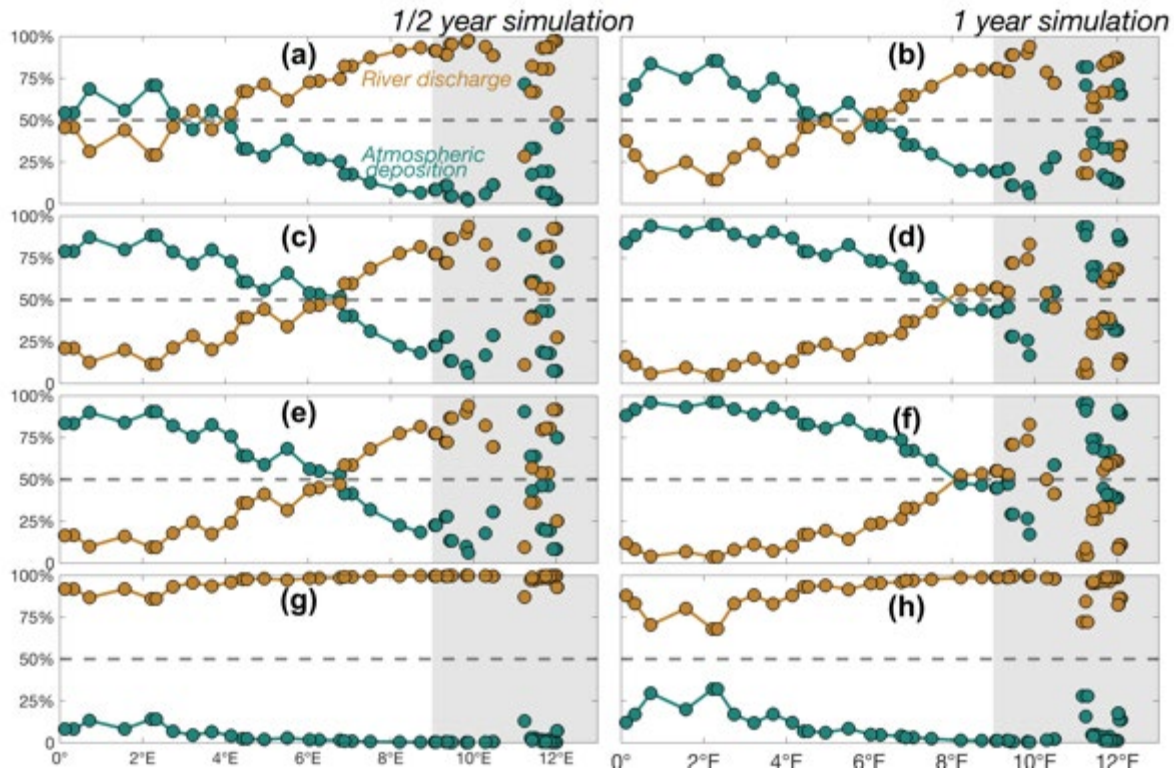

Figure 9. Sensitivity of the mechanisms driving gross dFe inputs to the Congo plume, accounting for seasonal variability in river discharge and atmospheric deposition along the GA08 transect under extreme conditions. Sensitivity tests use mean dFe input from atmospheric dFe deposition with riverine dFe input at maximum values in (a) and (b), and minimum values in (c) and (d); and average riverine dFe input with atmospheric dFe deposition input at maximum values in (e) and (f), and minimum values in (g) and (h). Left column show the contributions from the 1/2 year simulation and right column show the contributions from the 1 year simulation. The shelf region is shaded in grey.

4 Discussion

The Congo plume serves as an important source of freshwater and trace metals to the SAO. Along the 3°S GA08 cruise transect, elevated dFe concentrations were observed >1000 km from the Congo River mouth (~2.85 nM). This is despite approximately 96% of dFe being removed within 400 km from the Congo River mouth according to the dFe measurements in the Congo River (Vieira et al., 2020). Our investigation utilizing a particle tracking experiment explores the respective proportion of contributions from river discharge, atmospheric deposition, and sediment/submarine groundwater to the Congo plume based on three prior GA08 studies, which provide critical insight into the potential mechanisms that influence trace metals in the Congo plume (Vieira et al., 2020; Hunt et al., 2022; Liu et al., 2023). One proposed explanation for the source of offshore dFe is the contribution from river discharge, with sediment and/or submarine groundwater discharge inputs between river mouths and the Congo shelf zone being potential additional sources based on conservative ^{228}Ra budget analysis (Vieira et al., 2020). A subsequent study appears to conclusively eliminate one of these plausible dFe sources; the observation of an increasing Fe isotopic composition (δ^{56}Fe) from +0.33 to +0.94‰ with distance from the river mouth is contrary to the isotopically light (negative δ^{56}Fe) signature expected from shelf sediments (Chever et al., 2015; Klar et al., 2018) and sedimentary isotopically heavy δ^{56}Fe (Homoky et al., 2013; Fitzsimmons & Conway, 2023) decreasing from river to ocean. Instead, a more likely mechanism to sustain the high dFe concentrations and a heavy δ^{56}Fe signal is that dFe is bound by strong organic ligands. High discharge of elevated dissolved organic carbon (DOC) has been noted in the Congo River's key tributaries, e.g., Obangui and Ngoko-Sangha rivers in July and October, which coupled with a rapid lateral transport may contribute to the high off-shelf concentrations (Hunt et al., 2022).

Wet deposition has been proposed as a potential additional source to the Congo plume alongside riverine inputs (Liu et al., 2023) and this could also deliver dFe to the ocean in an organically-bound form (Kieber, 2001; Kieber, 2003; Willey et al., 2008), although, to our knowledge, the δ^{56}Fe signature of rain water is unknown. Budget analysis combining trace metals measurements in river, rainwater, and surface-ocean inputs to the Congo shelf suggested that wet deposition significantly contributed to the enrichment of certain metals such as Cd, Cu, Pb, and Zn in the Congo shelf zone at similar magnitude to Congo River inputs (Liu et al., 2023). Yet the gross contributions to Fe (0.02%), Co (5%), and Mn (8%) inventories appeared to be more limited in prior work (Liu et al., 2023). A direct comparison of gross inputs for dFe is however complicated by the removal factor of estuarine dFe. Mixing studies between river water and seawater almost invariably show rapid non-conservative removal of dFe (Bale & Morris, 1981; Mayer, 1982). Conversely, mixing studies between rain water and seawater appear to show a degree of dFe stability (Zhuang et al., 1995; Willey, 2005; Willey et al., 2008). Rain water could therefore be disproportionately more important than the above calculation suggests (by a factor of up to 100-

fold higher), although this would still only lead to a gross contribution of about 2%. This is not easily reconciled with the particle tracking work herein which appears to suggest much larger contributions. As we will discuss below however, there is a major difference in how these fluxes were calculated with respect to the area concerned which strongly affects the magnitude of the calculated riverine dFe inputs. Collectively, prior GA08 studies provide critical, complementary evidence regarding the contributors sustaining the trace metal Congo plume beyond river discharge from various perspectives.

Our particle tracking experiment has the capability to simulate dispersal of trace metals and the formation of the Congo plume in the absence of confounding biological/chemical processes. This is made possible by determining the number of particles released based on the dFe inputs from vertical transport (which implicitly includes sources from sediment and submarine groundwater over the shelf), atmospheric deposition, and river discharge assessed by regional measurements. By calculating the trajectory density for each source, the contributions of various processes to the Congo plume across the study area were distinguished and quantified. Specifically, we focused mainly on the dispersal of dFe in our experiments, as dFe is a crucial nutrient for phytoplankton growth and was identified to be least impacted by wet deposition in previous trace metal budget analyses (Liu et al., 2023).

Our findings substantiate the hypothesis that sources from sediment/submarine groundwater play a negligible role in the Congo plume (Hunt et al., 2022), primarily due to a negative/weak vertical flux within the plume region (Figures 1 and 4). Instead, river discharge and wet deposition significantly contribute to the trace metals enrichment in the Congo plume (Figure 6). This is consistent with the findings in (Liu et al., 2023). Moreover, wet deposition also significantly contributed to dFe input in the Congo shelf zone (Figure 6), apparently contradicting some lower estimates from prior analysis (Liu et al., 2023). One plausible explanation for this inconsistency could be attributed to differences in the riverine dFe concentrations used in the dFe flux budget analysis. The after-removal riverine dFe input (~11 nmol L^{-1}) used here was considerably lower compared to the measured dFe concentration in the Congo River (7385 nmol L^{-1}) used in Liu et al. (2023), which might also include a wet deposition component. Additionally, there is a critical difference in the calculation process compared to with prior work; herein we are referring to fluxes integrated or averaged across the whole Congo plume area, assuming to be 5×10^{12} m^2 as the freshwater plume (Hopkins et al., 2013). The dFe flux from the Congo River spread over the whole plume area is much smaller when normalized to the surface area of the plume than when concentrated in the inner shelf, with an area of 8.2×10^{10} m^2 (Liu et al., 2023). Therefore, by considering the riverine dFe concentration after estuarine removal processes (~11 nmol L^{-1}) and the whole average Congo plume area, our estimates suggest that the contribution of wet deposition could increase up to 47%. This is comparable to our estimate based on 1 year particle tracking experiment (~40%).

Our particle tracking experiments also have implications for understanding the spatial and temporal representativeness of the GA08 3°S section. The high cost of measuring trace metals at sea means that GEOTRACES cruises provide relatively sparse coverage and so it is important to consider how representative the obtained data sections are. If the cruise transects had occurred further south (3.5°S), the river-dominant zone would have been more constrained in the coastal regions. In contrast, a cruise with a transect further north (2.5°S) may have captured lower contributions of wet atmospheric deposition in the open ocean, due to a greater contribution of riverine input. The seasonal sensitivity analysis suggests the substantial contribution of riverine

and atmospheric inputs to the Congo Plume remains relatively robust and is less likely to vary with sampling date, despite variations in the boundary of the dominant zone (Figure 9). For instance, in scenarios where riverine input equals to the maximum riverine dFe input observed during December, river discharge dominates the region east of 6°E, while atmospheric deposition dominates the off-shelf zone westward of 3°E. Conversely, if the riverine input corresponds to the minimum riverine dFe input recorded in August, river discharge dominates the region east of 8°E and atmospheric deposition dominates the off-shelf zone westward of 6°E.

5 Conclusions

To identify and quantify the dominant sources of dFe within the Congo plume, we conducted particle tracking experiments based on measured dFe distributions to simulate and track the dispersal of dFe originating from river discharge, atmospheric deposition (mainly wet deposition), and vertical transport. Our dispersal simulations of river discharge input align with prior remote sensing observations of the Chl-a/low salinity plume, showing a consistent pattern of enhanced particle density in the plume region. In both simulations and satellite data, the Congo plume is characterized by a north-westward and west-southwestward extension from the river mouth. In the Congo plume region (mainly north of 6°S), both river discharge and atmospheric deposition are important sources of dFe, while vertical fluxes from depth are negligible. Quantitative comparison reveals that river discharge dominates as the dFe source in the shelf regions and parts of the open ocean north of 3°S, whereas atmospheric deposition dominates the other parts of open ocean north of 3°S and most regions south of 3°S, particularly for the 1 year simulations.

Specifically, along the 3°S transect of the GA08 cruise, the contribution of river discharge to the dFe in the Congo plume decreases from 90% to 30% westward from 9°E, and atmospheric deposition correspondingly increases from 10% to 70%. Over the Congo shelf zone, atmospheric deposition contributes around 20% to 40% of dFe, and could also be a major source of the dFe to the plume, particularly around the Congo River mouth (east of 11°E). Despite notable seasonality in atmospheric deposition and riverine dFe input, sensitivity analysis suggests a consistent pattern in terms of the dFe source to the plume when using mean dFe inputs, with patterns generally resulting from the conditions of lowest/highest river discharge inputs and highest atmospheric deposition input. Combined with the observations from GA08 cruise, our findings substantiate that atmospheric deposition, mainly in the form of wet deposition, is the major mechanism driving the enrichment of dFe, and likely other trace metals, in the region approximately 1000 km away from the Congo River mouth.

Acknowledgments

The authors thank the captain, crew and scientists of the R/V Meteor (GN08 cruise). Yuanyuan Gu was supported by the National Natural Science Foundation of China (42306222).

Data Availability Statement

OceanParcels is available at http://oceanparcels.org (Lange & van Sebille, 2017; Delandmeter & van Sebille, 2019) and the trace metal and nutrient data from GA08 cruise are obtained at PANGAEA: https://doi.pangaea.de/10.1594/ PANGAEA.947275 (Liu et al., 2022b).

ReferencesUncategorized References

Araujo, M., Noriega, C., & Lefèvre, N. (2014). Nutrients and carbon fluxes in the estuaries of major rivers flowing into the tropical Atlantic. *Frontiers in Marine Science*, *1*. https://doi.org/10.3389/fmars.2014.00010

Bale, A. J., & Morris, A. W. (1981). Laboratory simulation of chemical processes induced by estuarine mixing: The behaviour of iron and phosphate in estuaries. *Estuarine, Coastal and Shelf Science*, *13*(1), 1-10. https://doi.org/10.1016/s0302-3524(81)80101-6

Bordbar, M. H., Mohrholz, V., & Schmidt, M. (2021). The relation of wind-driven coastal and offshore upwelling in the Benguela Upwelling System. *Journal of Physical Oceanography*. https://doi.org/10.1175/jpo-d-20-0297.1

Boyle, E. A., Edmond, J. M., & Sholkovitz, E. R. (1977). The mechanism of iron removal in estuaries. *Geochimica et Cosmochimica Acta*, *41*(9), 1313-1324. https://doi.org/10.1016/0016-7037(77)90075-8

Browning, T. J., Achterberg, E. P., Engel, A., & Mawji, E. (2021). Manganese co-limitation of phytoplankton growth and major nutrient drawdown in the Southern Ocean. *Nature Communications*, *12*(1). https://doi.org/10.1038/s41467-021-21122-6

Browning, T. J., Achterberg, E. P., Rapp, I., Engel, A., Bertrand, E. M., Tagliabue, A., & Moore, C. M. (2017). Nutrient co-limitation at the boundary of an oceanic gyre. *Nature*, *551*(7679), 242-246. https://doi.org/10.1038/nature24063

Bruland, K. W., & Franks, R. P. (1983). Mn, Ni, Cu, Zn and Cd in the Western North Atlantic. In C. S. Wong, E. Boyle, K. W. Bruland, J. D. Burton, & E. D. Goldberg (Eds.), *Trace Metals in Sea Water* (pp. 395-414). Springer US. https://doi.org/10.1007/978-1-4757-6864-0_23

Capó, E., & McWilliams, J. C. (2022). Coherent Lagrangian Pathways Near an East Alboran Front. *Journal of Geophysical Research: Oceans*, *127*(3). https://doi.org/10.1029/2021jc018022

Carlson, R. R., Crowder, L. B., Martin, R. E., & Asner, G. P. (2024). The effect of reef morphology on coral recruitment at multiple spatial scales. *Proceedings of the National Academy of Sciences*, *121*(4). https://doi.org/10.1073/pnas.2311661121

Charette, M. A., Kipp, L. E., Jensen, L. T., Dabrowski, J. S., Whitmore, L. M., Fitzsimmons, J. N., Williford, T., Ulfsbo, A., Jones, E., Bundy, R. M., Vivancos, S. M., Pahnke, K., John, S. G., Xiang, Y., Hatta, M., Petrova, M. V., Heimbürger-Boavida, L. E., Bauch, D., Newton, R., . . . Zhang, R. (2020). The transpolar drift as a source of riverine and shelf-derived trace elements to the Central Arctic Ocean. *Journal of Geophysical Research: Oceans*, *125*(5). https://doi.org/10.1029/2019jc015920

Chelton, D. B., deSzoeke, R. A., Schlax, M. G., Naggar, K. E., & Siwertz, N. (1998). Geographical variability of the first baroclinic Rossby radius of deformation. *Journal of Physical Oceanography*, *28*(3), 433–460. https://doi.org/doi.org/10.1175/1520-0485(1998)028<0433:GVOTFB>2.0.CO;2

Chever, F., Rouxel, O. J., Croot, P. L., Ponzevera, E., Wuttig, K., & Auro, M. (2015). Total dissolvable and dissolved iron isotopes in the water column of the Peru upwelling regime. *Geochimica et Cosmochimica Acta*, *162*, 66-82. https://doi.org/10.1016/j.gca.2015.04.031

Coles, V. J., Brooks, M. T., Hopkins, J., Stukel, M. R., Yager, P. L., & Hood, R. R. (2013). The pathways and properties of the Amazon River Plume in the tropical North Atlantic

Ocean. *Journal of Geophysical Research: Oceans*, *118*(12), 6894-6913. https://doi.org/10.1002/2013jc008981

de Boyer Montégut, C. (2004). Mixed layer depth over the global ocean: An examination of profile data and a profile-based climatology. *Journal of Geophysical Research*, *109*(C12). https://doi.org/10.1029/2004jc002378

Delandmeter, P., & van Sebille, E. (2019). The Parcels v2.0 Lagrangian framework: new field interpolation schemes. *Geoscientific Model Development*, *12*(8), 3571-3584. https://doi.org/10.5194/gmd-12-3571-2019

Denamiel, C., Budgell, W. P., & Toumi, R. (2013). The Congo River plume: Impact of the forcing on the far-field and near-field dynamics. *Journal of Geophysical Research: Oceans*, *118*(2), 964-989. https://doi.org/10.1002/jgrc.20062

Duinker, J. C., & Nolting, R. F. (1976). Distribution model for particulate trace metals in the rhine estuary, Southern Bight and Dutch Wadden Sea. *Netherlands Journal of Sea Research*, *10*(1), 71-102. https://doi.org/10.1016/0077-7579(76)90005-3

Dunckley, J. F., Koseff, J. R., Steinbuck, J. V., Monismith, S. G., & Genin, A. (2012). Comparison of mixing efficiency and vertical diffusivity models from temperature microstructure. *Journal of Geophysical Research: Oceans*, *117*(C10). https://doi.org/10.1029/2012jc007967

Eddebbar, Y. A., Subramanian, A. C., Whitt, D. B., Long, M. C., Verdy, A., Mazloff, M. R., & Merrifield, M. A. (2021). Seasonal modulation of dissolved oxygen in the equatorial Pacific by tropical instability vortices. *Journal of Geophysical Research: Oceans*, *126*(11). https://doi.org/10.1029/2021jc017567

Fitzsimmons, J. N., & Conway, T. M. (2023). Novel Insights into Marine Iron Biogeochemistry from Iron Isotopes. *Ann Rev Mar Sci*, *15*, 383-406. https://doi.org/10.1146/annurev-marine-032822-103431

Frank, M., Achterberg, E. P., Bristow, L. A., Browning, T. J., Deng, F., Handmann, P. V. K., Hathorne, E. C., Hopwood, M. J., Lodeiro, P., Menzel-Barraqueta, J.-L., Merschel, G., Meyer, S., Baro, J. P., Rahlf, P., Rath, W., Schlosser, C., Stippkugel, A., Vieira, L. H., Zitoun, R., & Raeke, A. (2016). Trace metal chemistry in the water column of the Angola basin - A Contribution to the international GEOTRACES program - cruise No. M121, November 22, – December 27, 2015, Walvis Bay (Namibia) – Walvis Bay (Namibia).

Gledhill, M., & Buck, K. N. (2012). The organic complexation of iron in the marine environment: a review. *Front Microbiol*, *3*, 69. https://doi.org/10.3389/fmicb.2012.00069

GLORYS12V1. Marine Data Store (MDS). https://doi.org/10.48670/moi-00021

Gordon, A. L., & Bosley, K. T. (1991). Cyclonic gyre in the tropical South Atlantic. *Deep Sea Research Part A. Oceanographic Research Papers*, *38*, S323-S343. https://doi.org/10.1016/s0198-0149(12)80015-x

Guieu, C., Bonnet, S., Wagener, T., & Loÿe-Pilot, M.-D. (2005). Biomass burning as a source of dissolved iron to the open ocean? *Geophysical Research Letters*, *32*(19), n/a-n/a. https://doi.org/10.1029/2005gl022962

Gustafsson, Ö., Widerlund, A., Andersson, P. S., Ingri, J., Roos, P., & Ledin, A. (2000). Colloid dynamics and transport of major elements through a boreal river — brackish bay mixing zone. *Marine Chemistry*, *71*(1-2), 1-21. https://doi.org/10.1016/s0304-4203(00)00035-9

Hatta, M., Measures, C. I., Wu, J., Roshan, S., Fitzsimmons, J. N., Sedwick, P., & Morton, P. (2015). An overview of dissolved Fe and Mn distributions during the 2010–2011 U.S. GEOTRACES north Atlantic cruises: GEOTRACES GA03. *Deep Sea Research Part II: Topical Studies in Oceanography*, *116*, 117-129. https://doi.org/10.1016/j.dsr2.2014.07.005

Hersbach, H., Bell, B., Berrisford, P., Biavati, G., Horányi, A., Muñoz Sabater, J., Nicolas, J., Peubey, C., Radu, R., Rozum, I., Schepers, D., Simmons, A., Soci, C., Dee, D., & Thépaut, J.-N. (2023). *ERA5 hourly data on single levels from 1940 to present. Copernicus Climate Change Service (C3S) Climate Data Store (CDS),* . https://doi.org/10.24381/cds.adbb2d47 (Accessed on 04-04-2022)

Holliday, L. M., & Liss, P. S. (1976). The behaviour of dissolved iron, manganese and zinc in the Beaulieu Estuary, S. England. *Estuarine and Coastal Marine Science*, *4*(3), 349-353. https://doi.org/10.1016/0302-3524(76)90066-9

Homoky, W. B., John, S. G., Conway, T. M., & Mills, R. A. (2013). Distinct iron isotopic signatures and supply from marine sediment dissolution. *Nat Commun*, *4*, 2143. https://doi.org/10.1038/ncomms3143

Hong, H., & Kester, D. R. (1986). Redox state of iron in the offshore waters of Peru. *Limnology Oceanography*, *31*(3), 512-524. https://doi.org/10.4319/lo.1986.31.3.0512

Hopkins, J., Lucas, M., Dufau, C., Sutton, M., Stum, J., Lauret, O., & Channelliere, C. (2013). Detection and variability of the Congo River plume from satellite derived sea surface temperature, salinity, ocean colour and sea level. *Remote Sensing of Environment*, *139*, 365-385. https://doi.org/10.1016/j.rse.2013.08.015

Hopkins, J., & Polton, J. A. (2011). Scales and structure of frontal adjustment and freshwater export in a region of freshwater influence. *Ocean Dynamics*, *62*(1), 45-62. https://doi.org/10.1007/s10236-011-0475-7

Hsieh, Y.-T., Geibert, W., Woodward, E. M. S., Wyatt, N. J., Lohan, M. C., Achterberg, E. P., & Henderson, G. M. (2021). Radium-228-derived ocean mixing and trace element inputs in the South Atlantic. *Biogeosciences*, *18*(5), 1645-1671. https://doi.org/10.5194/bg-18-1645-2021

Hunt, H. R., Summers, B. A., Sieber, M., Krisch, S., Al-Hashem, A., Hopwood, M., Achterberg, E. P., & Conway, T. M. (2022). Distinguishing the influence of sediments, the Congo River, and water-mass mixing on the distribution of iron and its isotopes in the Southeast Atlantic Ocean. *Marine Chemistry*, *247*. https://doi.org/10.1016/j.marchem.2022.104181

Jickells, T. D., An, Z. S., Andersen, K. K., Baker, A. R., Bergametti, G., Brooks, N., Cao, J. J., Boyd, P. W., Duce, R. A., Hunter, K. A., Kawahata, H., Kubilay, N., laRoche, J., Liss, P. S., Mahowald, N., Prospero, J. M., Ridgwell, A. J., Tegen, I., & Torres, R. (2005). Global iron connections between desert dust, ocean biogeochemistry, and climate. *Science*, *308*(5718), 67-71. https://doi.org/10.1126/science.1105959

Kieber, R. J. (2003). Temporal variability of rainwater iron speciation at the Bermuda Atlantic Time Series Station. *Journal of Geophysical Research*, *108*(C8). https://doi.org/10.1029/2001jc001031

Kieber, R. J., Williams, K., Willey, J. D., Skrabal, S., Avery, G. B. (2001). Iron speciation in coastal rainwater: Concentration and deposition to seawater. *Mar. Chem.* , *73*, 83–95. https://doi.org/10.1016/S0304-4203(00)00097-9

Klar, J. K., Schlosser, C., Milton, J. A., Woodward, E. M. S., Lacan, F., Parkinson, I. J., Achterberg, E. P., & James, R. H. (2018). Sources of dissolved iron to oxygen minimum zone waters on the Senegalese continental margin in the tropical North Atlantic Ocean: Insights from iron isotopes. *Geochimica et Cosmochimica Acta*, *236*, 60-78. https://doi.org/10.1016/j.gca.2018.02.031

Klunder, M. B., Laan, P., Middag, R., Baar, H. J. W. d., & Bakker, K. (2012). Dissolved iron measurements from 32 stations in the Central Arctic Ocean and Arctic Shelf Sea during POLARSTERN expedition ARK-XXII/2.

Krachler, R., Jirsa, F., & Ayromlou, S. (2005). Factors influencing the dissolved iron input by river water to the open ocean. *Biogeosciences*, *2*(4), 311-315. https://doi.org/10.5194/bg-2-311-2005

Krachler, R., Krachler, R. F., von der Kammer, F., Süphandag, A., Jirsa, F., Ayromlou, S., Hofmann, T., & Keppler, B. K. (2010). Relevance of peat-draining rivers for the riverine input of dissolved iron into the ocean. *Science of The Total Environment*, *408*(11), 2402-2408. https://doi.org/10.1016/j.scitotenv.2010.02.018

Lange, M., & van Sebille, E. (2017). Parcels v0.9: prototyping a Lagrangian ocean analysis framework for the petascale age. *Geoscientific Model Development*, *10*(11), 4175-4186. https://doi.org/10.5194/gmd-10-4175-2017

Laraque, A., Moukandi N'kaya, G. D., Orange, D., Tshimanga, R., Tshitenge, J. M., Mahé, G., Nguimalet, C. R., Trigg, M. A., Yepez, S., & Gulemvuga, G. (2020). Recent budget of hydroclimatology and hydrosedimentology of the Congo River in Central Africa. *Water*, *12*(9). https://doi.org/10.3390/w12092613

Ledwell, J. R., Watson, A. J., & Law, C. S. (1993). Evidence for slow mixing across the pycnocline from an open-ocean tracer-release experiment. *Nature*, *364*(6439), 701-703. https://doi.org/10.1038/364701a0

Liu, T., Hopwood, M. J., Krisch, S., Vieira, L. H., & Achterberg, E. P. (2023). Trace metal fluxes of Cd, Cu, Pb and Zn From the Congo River into the South Atlantic Ocean Are supplemented by atmospheric inputs. *Geophysical Research Letters*, *50*(24). https://doi.org/10.1029/2023gl107150

Liu, T., Krisch, S., Hopwood, M. J., Achterberg, E. P., & Mutzberg, A. (2022b). Trace metal data from water samples during METEOR cruise M121. *PANGAEA*. https://doi.org/https://doi.org/10.1594/PANGAEA.947275

Liu, T., Krisch, S., Xie, R. C., Hopwood, M. J., Dengler, M., & Achterberg, E. P. (2022a). Sediment release in the Benguela Upwelling System dominates trace metal input to the shelf and Eastern South Atlantic Ocean. *Global Biogeochemical Cycles*, *36*(9). https://doi.org/10.1029/2022gb007466

Martin, A. P., Lucas, M. I., Painter, S. C., Pidcock, R., Prandke, H., Prandke, H., & Stinchcombe, M. C. (2010). The supply of nutrients due to vertical turbulent mixing: A study at the Porcupine Abyssal Plain study site in the northeast Atlantic. *Deep Sea Research Part II: Topical Studies in Oceanography*, *57*(15), 1293-1302. https://doi.org/10.1016/j.dsr2.2010.01.006

Martin, J. H., Coale, K. H., Johnson, K. S., Fitzwater, S. E., Gordon, R. M., Tanner, S. J., Hunter, C. N., Elrod, V. A., Nowicki, J. L., Coley, T. L., Barber, R. T., Lindley, S., Watson, A. J., Van Scoy, K., Law, C. S., Liddicoat, M. I., Ling, R., Stanton, T., Stockel, J., . . . Tindale, N. W.

(1994). Testing the iron hypothesis in ecosystems of the equatorial Pacific Ocean. *Nature*, *371*(6493), 123-129. https://doi.org/10.1038/371123a0

Martin, J. H., Fitzwater, S. E., & Gordon, R. M. (1990). Iron deficiency limits phytoplankton growth in Antarctic waters. *Global Biogeochemical Cycles*, *4*(1), 5-12. https://doi.org/10.1029/GB004i001p00005

Martins, M. S., & Stammer, D. (2022). Interannual variability of the Congo River Plume-induced sea surface salinity. *Remote Sensing*, *14*(4). https://doi.org/10.3390/rs14041013

Mayer, L. M. (1982). Aggregation of colloidal iron during estuarine mixing: Kinetics, mechanism, and seasonality. *Geochimica et Cosmochimica Acta*, *46*(12), 2527-2535. https://doi.org/10.1016/0016-7037(82)90375-1

Measures, C. I., & Brown, E. T. (1996). Estimating Dust Input to the Atlantic Ocean Using Surface Water Aluminium Concentrations. In S. Guerzoni & R. Chester (Eds.), *The Impact of Desert Dust Across the Mediterranean* (pp. 301-311). Springer Netherlands. https://doi.org/10.1007/978-94-017-3354-0_30

Mignard, S. L.-A., Mulder, T., Martinez, P., Charlier, K., Rossignol, L., & Garlan, T. (2017). Deep-sea terrigenous organic carbon transfer and accumulation: Impact of sea-level variations and sedimentation processes off the Ogooue River (Gabon). *Marine and Petroleum Geology*, *85*, 35-53. https://doi.org/10.1016/j.marpetgeo.2017.04.009

Millero, F. J. (1998). Solubility of Fe(III) in seawater. *Earth and Planetary Science Letters*, *154*(1-4), 323-329. https://doi.org/10.1016/s0012-821x(97)00179-9

Missirlis, F., Rijkenberg, M. J. A., Middag, R., Laan, P., Gerringa, L. J. A., van Aken, H. M., Schoemann, V., de Jong, J. T. M., & de Baar, H. J. W. (2014). The distribution of dissolved iron in the West Atlantic Ocean. *PLoS One*, *9*(6). https://doi.org/10.1371/journal.pone.0101323

Moore, C. M., Mills, M. M., Arrigo, K. R., Berman-Frank, I., Bopp, L., Boyd, P. W., Galbraith, E. D., Geider, R. J., Guieu, C., Jaccard, S. L., Jickells, T. D., La Roche, J., Lenton, T. M., Mahowald, N. M., Marañón, E., Marinov, I., Moore, J. K., Nakatsuka, T., Oschlies, A., . . . Ulloa, O. (2013). Processes and patterns of oceanic nutrient limitation. *Nature Geoscience*, *6*(9), 701-710. https://doi.org/10.1038/ngeo1765

Noble, A. E., Lamborg, C. H., Ohnemus, D. C., Lam, P. J., Goepfert, T. J., Measures, C. I., Frame, C. H., Casciotti, K. L., DiTullio, G. R., Jennings, J., & Saito, M. A. (2012). Basin-scale inputs of cobalt, iron, and manganese from the Benguela-Angola front to the South Atlantic Ocean. *Limnology and Oceanography*, *57*(4), 989-1010. https://doi.org/10.4319/lo.2012.57.4.0989

Powell, R. T., & Wilson-Finelli, A. (2003). Importance of organic Fe complexing ligands in the Mississippi River plume. *Estuarine, Coastal and Shelf Science*, *58*(4), 757-763. https://doi.org/10.1016/s0272-7714(03)00182-3

Rapp, I., Schlosser, C., Menzel Barraqueta, J.-L., Wenzel, B., Lüdke, J., Scholten, J., Gasser, B., Reichert, P., Gledhill, M., Dengler, M., & Achterberg, E. P. (2019). Controls on redox-sensitive trace metals in the Mauritanian oxygen minimum zone. *Biogeosciences*, *16*(21), 4157-4182. https://doi.org/10.5194/bg-16-4157-2019

Rigby, S. J., Williams, R. G., Achterberg, E. P., & Tagliabue, A. (2020). Resource availability and entrainment are driven by offsets between nutriclines and winter mixed-layer depth. *Global Biogeochemical Cycles*, *34*(7). https://doi.org/10.1029/2019gb006497

Rudnick, R. L., & Gao, S. (2014). Composition of the Continental Crust. In *Treatise on Geochemistry* (pp. 1-51). https://doi.org/10.1016/b978-0-08-095975-7.00301-6

Schulz, M., Prospero, J. M., Baker, A. R., Dentener, F., Ickes, L., Liss, P. S., Mahowald, N. M., Nickovic, S., Garcia-Pando, C. P., Rodriguez, S., Sarin, M., Tegen, I., & Duce, R. A. (2012). Atmospheric transport and deposition of mineral dust to the ocean: implications for research needs. *Environ Sci Technol*, *46*(19), 10390-10404. https://doi.org/10.1021/es300073u

Seijo-Ellis, G., Giglio, D., & Salmun, H. (2023). Intrusions of Amazon River Waters in the Virgin Islands Basin During 2007–2017. *Journal of Geophysical Research: Oceans*, *128*(3). https://doi.org/10.1029/2022jc018709

Severmann, S., McManus, J., Berelson, W. M., & Hammond, D. E. (2010). The continental shelf benthic iron flux and its isotope composition. *Geochimica et Cosmochimica Acta*, *74*(14), 3984-4004. https://doi.org/10.1016/j.gca.2010.04.022

Shelley, R. U., Roca-Martí, M., Castrillejo, M., Sanial, V., Masqué, P., Landing, W. M., van Beek, P., Planquette, H., & Sarthou, G. (2017). Quantification of trace element atmospheric deposition fluxes to the Atlantic Ocean (>40°N; GEOVIDE, GEOTRACES GA01) during spring 2014. *Deep Sea Research Part I: Oceanographic Research Papers*, *119*, 34-49. https://doi.org/10.1016/j.dsr.2016.11.010

Sholkovitz, E., Boyle, E., & Price, N. (1978). The removal of dissolved humic acids and iron during estuarine mixing. *Earth and Planetary Science Letters*, *40*(1), 130-136. https://doi.org/10.1016/0012-821x(78)90082-1

Signorini, S. R., Murtugudde, R. G., McClain, C. R., Christian, J. R., Picaut, J., & Busalacchi, A. J. (1999). Biological and physical signatures in the tropical and subtropical Atlantic. *Journal of Geophysical Research: Oceans*, *104*(C8), 18367-18382. https://doi.org/10.1029/1999jc900134

Steinfeldt, R., Sültenfuß, J., Dengler, M., Fischer, T., & Rhein, M. (2015). Coastal upwelling off Peru and Mauritania inferred from helium isotope disequilibrium. *Biogeosciences*, *12*(24), 7519-7533. https://doi.org/10.5194/bg-12-7519-2015

Su, H., Yang, R., Zhang, A., & Li, Y. (2015). Dissolved iron distribution and organic complexation in the coastal waters of the East China Sea. *Marine Chemistry*, *173*, 208-221. https://doi.org/10.1016/j.marchem.2015.03.007

Tagliabue, A. (2019). Elemental Distribution: Overview. In H. J. B. In J. K. Cochran, & P. L. Yager (Ed.), *Encyclopedia of Ocean Sciences* (3rd ed., Vol. 1). (London: Elsevier)

Tagliabue, A., Aumont, O., DeAth, R., Dunne, J. P., Dutkiewicz, S., Galbraith, E., Misumi, K., Moore, J. K., Ridgwell, A., Sherman, E., Stock, C., Vichi, M., Völker, C., & Yool, A. (2016). How well do global ocean biogeochemistry models simulate dissolved iron distributions? *Global Biogeochemical Cycles*, *30*(2), 149-174. https://doi.org/10.1002/2015gb005289

Tanhua, T., & Liu, M. (2015). Upwelling velocity and ventilation in the Mauritanian upwelling system estimated by CFC-12 and SF6 observations. *Journal of Marine Systems*, *151*, 57-70. https://doi.org/10.1016/j.jmarsys.2015.07.002

Theodosi, C., Markaki, Z., & Mihalopoulos, N. (2010). Iron speciation, solubility and temporal variability in wet and dry deposition in the Eastern Mediterranean. *Marine Chemistry*, *120*(1-4), 100-107. https://doi.org/10.1016/j.marchem.2008.05.004

Tonnard, M., Planquette, H., Bowie, A. R., van der Merwe, P., Gallinari, M., Desprez de Gésincourt, F., Germain, Y., Gourain, A., Benetti, M., Reverdin, G., Tréguer, P., Boutorh, J., Cheize, M., Lacan, F., Menzel Barraqueta, J.-L., Pereira-Contreira, L., Shelley, R., Lherminier, P., & Sarthou, G. (2020). Dissolved iron in the North Atlantic Ocean and Labrador Sea along the GEOVIDE section (GEOTRACES section GA01). *Biogeosciences*, *17*(4), 917-943. https://doi.org/10.5194/bg-17-917-2020

Vieira, L. H., Krisch, S., Hopwood, M. J., Beck, A. J., Scholten, J., Liebetrau, V., & Achterberg, E. P. (2020). Unprecedented Fe delivery from the Congo River margin to the South Atlantic Gyre. *Nat Commun*, *11*(1), 556. https://doi.org/10.1038/s41467-019-14255-2

Walker, N. D., Wiseman, W. J., Rouse, L. J., & Babin, A. (2005). Effects of river discharge, wind dtress, and slope eddies on circulation and the satellite-observed structure of the Mississippi River Plume. *Journal of Coastal Research*, *216*, 1228-1244. https://doi.org/10.2112/04-0347.1

Willey, J. D., Kieber, R. J., Seaton, P. J., & Miller, C. (2008). Rainwater as a source of Fe(II)-stabilizing ligands to seawater. *Limnology and Oceanography*, *53*(4), 1678-1684. https://doi.org/10.4319/lo.2008.53.4.1678

Willey, J. D., Kieber, R. J., Williams, K. H., Crozier, J. S., Skrabal, S. A., and Avery, G. B. (2000). Temporal variability of iron speciation in coastal rainwater. *J. Atmos. Chem.*, *37*, 185–205. https://doi.org/https://doi.org/10.1023/a:1006421624865

Willey, J. D., Whitehead, R. F., Kieber, R. J., and Hardison, D. R. (2005). Oxidation of Fe(II) in Rainwater. *Environ. Sci. Technol.*, *39*, 2579–2585. https://doi.org/https://doi.org/10.1021/es0404522

Xu, H., & Weber, T. (2021). Ocean dust deposition rates constrained in a data-assimilation model of the marine aluminum cycle. *Global Biogeochemical Cycles*, *35*(9). https://doi.org/10.1029/2021gb007049

Youngs, M. K., Freilich, M. A., & Lovenduski, N. S. (2023). Air-sea CO2 fluxes localized by topography in a Southern Ocean channel. *Geophysical Research Letters*, *50*(18). https://doi.org/10.1029/2023gl104802

Yücel, M., Gartman, A., Chan, C. S., & Luther, G. W. (2011). Hydrothermal vents as a kinetically stable source of iron-sulphide-bearing nanoparticles to the ocean. *Nature Geoscience*, *4*(6), 367-371. https://doi.org/10.1038/ngeo1148

Zhuang, G., Yi, Z., & Wallace, G. T. (1995). Iron(II) in rainwater, snow, and surface seawater from a coastal environment. *Marine Chemistry*, *50*(1-4), 41-50. https://doi.org/10.1016/0304-4203(95)00025-m